Engineering Failure Analysis 33 (2013) 236–250

Contents lists available at SciVerse ScienceDirect

Engineering Failure Analysis

journal homepage: www.elsevier.com/locate/engfailanal

Heterogeneous materials in compression: Correlations between absorbed, released and acoustic emission energies

A. Carpinteri, M. Corrado *, G. Lacidogna

Politecnico di Torino, Department of Structural, Geotechnical and Building Engineering, Corso Duca degli Abruzzi 24, 10129 Torino, Italy

ARTICLE INFO

Article history:
Received 10 April 2012
Received in revised form 26 April 2013
Accepted 27 May 2013
Available online 4 June 2013

Keywords:
Quasi-brittle materials
Acoustic emission
Compression test
Brittle fracture
Energy release

ABSTRACT

Compression tests on concrete and rocks – limestone, marble and granite – specimens have been carried out to investigate on the correlation between absorbed, released and acoustic emission energies. To this aim, the complete load vs. displacement curves have been obtained up to complete failure, evidencing very different post-peak responses – variable from normal softening to catastrophic snap-back – by varying the material, even for the same size and slenderness. Due to the expected brittle behaviour of some of the considered specimens, the loading process has been controlled by means of the circumferential strain with a linked chain placed around the cylindrical specimen at mid-height. The absorbed energy per unit surface is then computed through the overlapping constitutive law. Such a parameter, that results to be almost scale-invariant, is compared to the elastic energy accumulated in the body at the point of instability to define a structural brittleness index. Furthermore, all the tests have been monitored by means of the acoustic emission technique. The obtained data have been analysed in details, in order to draw a connection with the released energy in the post-peak regime, and to discriminate the different failure mechanisms.

1. Introduction

Damage and fracture characterising the compressive failure of heterogeneous materials such as rocks and concrete are complex processes involving wide ranges of time and length scales, from the micro- to the structural-scale. They are governed by the nucleation, growth and coalescence of microcracks and defects, eventually leading to the final collapse, and to the loss of the classical mechanical parameters, such as nominal strength, dissipated energy density and deformation at failure, as material properties [1]. Furthermore, the collapse mechanism strongly depends on the evolution of the cracking pattern during the loading process. Typically, crushing collapse is expected for very stocky specimens, shear failure with the development of inclined slip bands for intermediate values of slenderness, and splitting for very slender samples. Such a variety of failure mechanisms makes the definition of scale-invariant constitutive laws in compression difficult to be achieved. However, several experimental results [2,5] have evidenced that the post-peak regime is characterised by a strong strain localisation, independently of the actual failure mechanism. Consequently, in the softening regime, the energy dissipation results to be a surface-dominated phenomenon, analogously to the tensile behaviour. Such evidences have been profitably used to define a constitutive model for quasi-brittle materials in compression, namely the Overlapping Crack Model (OCM) [6]. The main assumption of the OCM is that the localisation process, whatever may be its origin, is modelled by means of a fictitious interpenetration of the two parts of the specimen, that exhibit an elastic behaviour. Accordingly, all

* Corresponding author. Tel.: +39 011 0904858; fax: +39 0110904899.
E-mail address: mauro.corrado@polito.it (M. Corrado).

1350-6307/$ - see front matter © 2013 Elsevier Ltd. All rights reserved.
http://dx.doi.org/10.1016/j.engfailanal.2013.05.016

the energy dissipation takes place over the interpenetration surface. An extensive application of such a simple model to concrete-like materials in uniaxial and eccentric compression tests has permitted to explain the well-known size and slenderness effects on the structural ductility [6,7]. In particular, it has been demonstrated that the stability of the overall behaviour can be correctly predicted by means of a dimensionless number function of geometrical (size and slenderness) and mechanical parameters (crushing energy, compressive strength and ultimate strain).

The OCM has been proved to be very effective in describing the overall behaviour of specimens in compression, without going into the details of the cracking pattern, as well as in determining the amount of dissipated energy during the complete loading process. On the other hand, more information on the modalities of energy release and the development of cracking patterns can be obtained from the acoustic emission (AE) monitoring technique. The application of piezoelectric transducers to the surface of the structural elements, in fact, permits to detect the elastic waves propagating within the bulk material, induced by the crack formation and propagation. This technique is largely used for the diagnosis of structural damage phenomena occurring in concrete and rock structures [8–10], as well as for detecting cracks and plastic deformations in metals [11]. Recently, AE data have been interpreted by means of statistical and fractal analysis, considering the multi-scale aspect of cracking phenomena [12], showing that the energy release, proportional to the cumulative number of AE events, is a surface-dominated phenomenon. Analogously, also the localisation of cracks distribution within the specimen volume by means of the AE technique has physically confirmed the localisation of the energy dissipation over preferential bands and surfaces during the damage evolution [13–15]. Furthermore, a detailed analysis of the shape of the AE waves recorded during the tests permits the different types of failure to be identified [8–10,16,17]. The AE parameters, such as the frequency, the rise time and the peak amplitude, in fact, strictly depend on the specimen damage, making possible to discriminate shear cracking from tensile cracking processes.

In the present paper, experimental results of compression tests carried out on cylindrical specimens of different types of rock and concrete, are analysed from the point of view of the balance between stored, released and absorbed energy during the complete loading process. The stability of the loading process is also investigated, and described on the basis of a dimensionless number, function of mechanical and geometrical parameters. Furthermore, the AE monitoring technique has been applied to all the tests, and the obtained data are put into relation with the released energy, and further analysed to identify the prevailing failure mechanism by varying the specimen geometry.

2. Scale independent constitutive laws

Damage localisation strongly affects the behaviour of heterogeneous materials in compression, with particular regard to the post-peak regime [2–5]. As a result, it is well-established that the classical stress vs. strain constitutive laws, which assume a homogeneous response along the specimen axis are strongly affected by the size and the slenderness of the specimen. They are commonly used for design purposes, though are completely ineffective in describing complex mechanical behaviours, such as the ductile-to-brittle transition by varying the structural scale. A significant step toward the definition of a scale independent constitutive law for quasi-brittle materials has been done by Carpinteri et al. [6], with the proposal of the Overlapping Crack Model. Based on the original experimental insight by Kotsovos [3], and van Mier [4], the proposed model describes the inelastic deformation due to material damage in the post-peak softening regime by means of a fictitious interpenetration, while the bulk material undergoes an elastic unloading. Accordingly, a couple of constitutive laws are introduced in compression, in close analogy with the Cohesive Crack Model: a reversible stress vs. strain relationship for the bulk material (Fig. 1a), and a stress vs. displacement (overlapping) relationship for the damage band (Fig. 1b). The latter law describes how the stress in the damaged material decreases from the compressive strength, σ_c, up to a residual value, σ_r, by increasing the interpenetration displacement. Such a model provides that the energy dissipation in the post-peak regime takes place within the damage band. The area below the stress–overlapping displacement curve of Fig. 1b represents the crushing energy per surface unit, G_C, which can be assumed as a size-independent material property. The main advantage

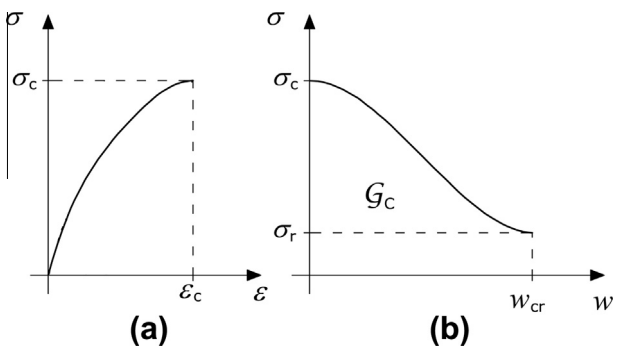

Fig. 1. Overlapping Crack Model: (a) pre-peak stress–strain diagram; (b) post-peak stress–overlapping displacement law.

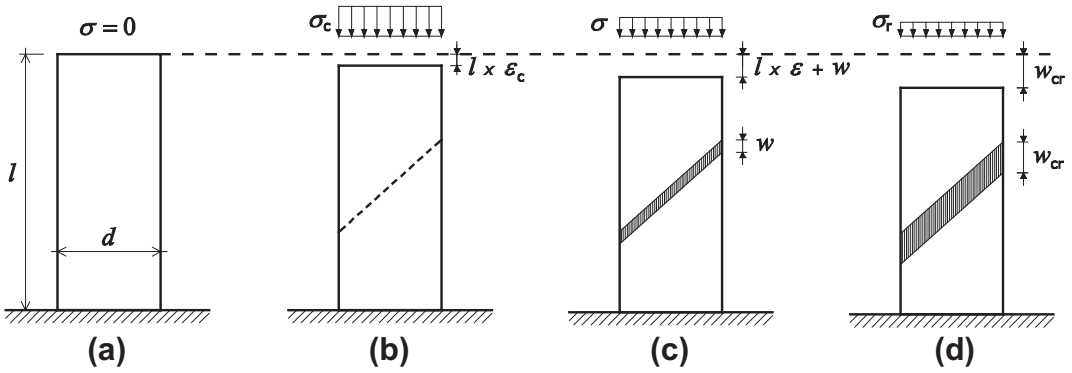

Fig. 2. Subsequent stages in the deformation history of a specimen in compression.

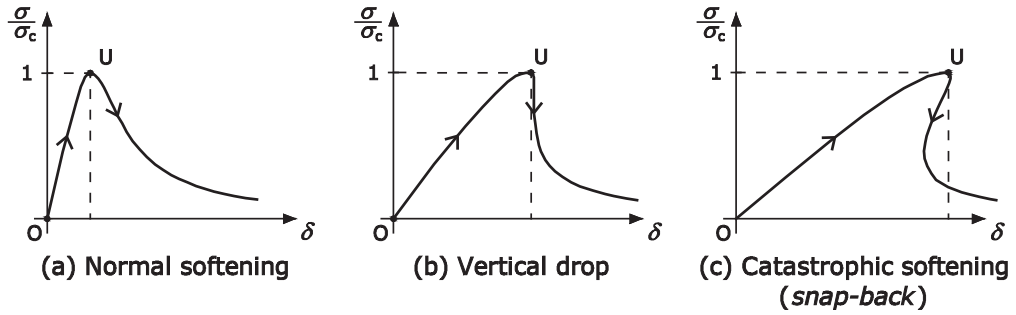

Fig. 3. Stress–displacement response of a specimen in compression.

of such a law is that it can be derived from the experimental test on a specimen of a generic size, and then it can be applied to every other sizes.

Let us consider the specimen subjected to uniaxial compression test shown in Fig. 2. The application of the OCM permits the mechanical response to be represented by three subsequent phases. A first stage where the behaviour is mainly characterised by the elastic modulus of the material: a simple linear elastic stress–strain law can be assumed, or even more complicated nonlinear relationships taking into account energy dissipation within the volume due to initiation and propagation of microcracks (see Fig. 2b). By approaching the compressive strength, such microcracks interact forming macrocracks, and, eventually, localising on a preferential surface. A second stage where, after reaching the ultimate compressive strength, σ_c, the inelastic deformations are localised in a crushing band. The behaviour of this zone is described by the softening law shown in Fig. 1b, whereas the bulk material still behaves elastically (see Fig. 2c). The total shortening of the specimen can be computed as the sum of the elastic deformation and the interpenetration displacement w:

$$\delta = \varepsilon l + w; \text{for } w < w_{cr}, \tag{1}$$

where l is the specimen length. Both the contributions ε and w can be expressed as a function of the stress level, according to the corresponding constitutive laws shown in Fig. 1. While the crushing zone overlaps, the elastic zone expands at progressively decreasing stresses. When $\delta \geqslant w_{cr}$, in the third stage, the material in the crushing zone is completely damaged and is able to transfer only a constant residual stress, σ_r (see Fig. 2d). As a result, the transition from softening to snap-back instability in the load vs. displacement global response, experimentally obtained by increasing the specimen slenderness and/or by varying the mechanical properties, can be correctly predicted. In particular, the softening process is stable under displacement control, only when the slope $d\delta/d\sigma$ in the post-peak regime is negative (Fig. 3a). On the contrary, the snap-back instability is obtained when the slope $d\delta/d\sigma$ of the softening branch becomes positive, Fig. 3c. In this case, the virtual snap-back branch can be experimentally captured only if the loading process is controlled by means of a monotonic increasing function of time. Usually, the circumferential expansion can be used. From a practical point of view, it can be detected by means of an extensometer attached at the ends of a linked chain with rollers placed around the cylindrical specimen, at mid-height. However, when the slenderness is larger than 3, the failure does not always occur at the middle of the specimen and, therefore, the circumferential expansion at mid-height is no longer a stable parameter during the loading process. In these cases, an alternative method of feedback control can be based on the inelastic part of the total deformation, has originally proposed by Okubo and Nishimatsu [18], and later applied by others. In accordance with the study on the stability of the loading process proposed by the authors in [7], a catastrophic softening (snap-back) occurs when:

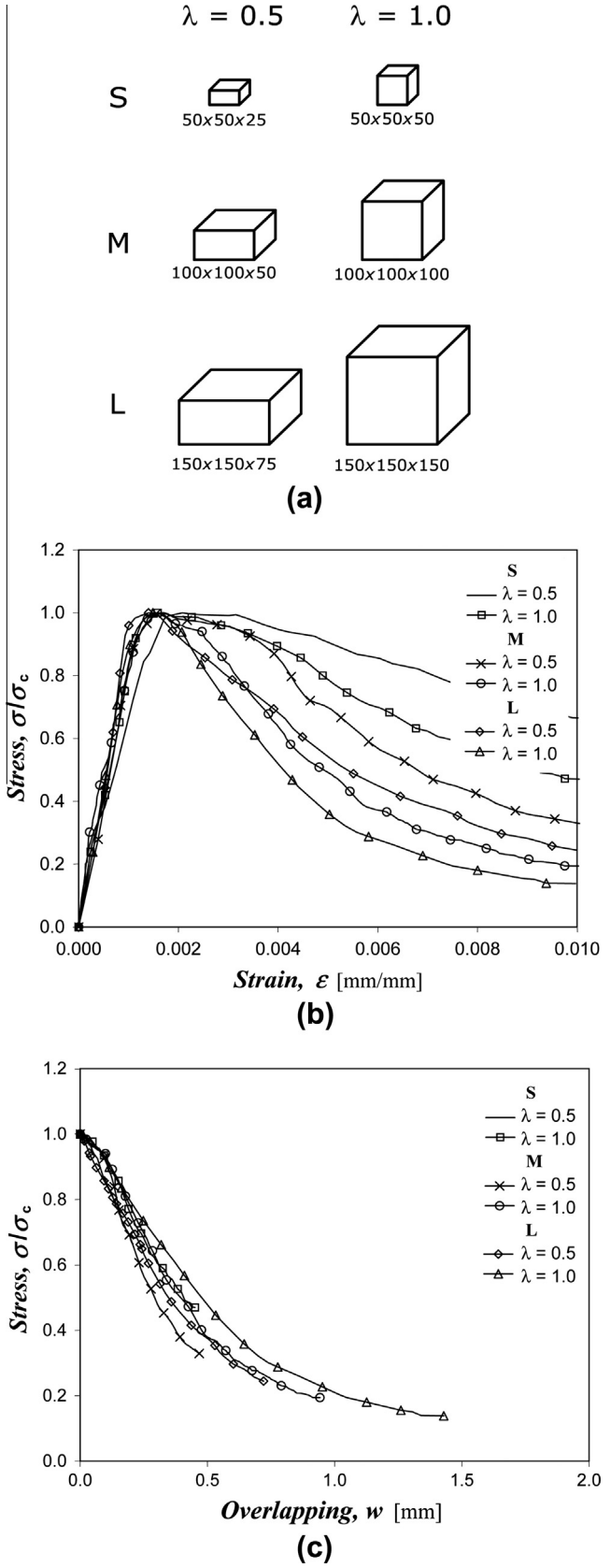

Fig. 4. Compression tests on concrete specimens by Ferrara and Gobbi [19] (a); stress vs. strain diagrams (b); overlapping law diagrams (c).

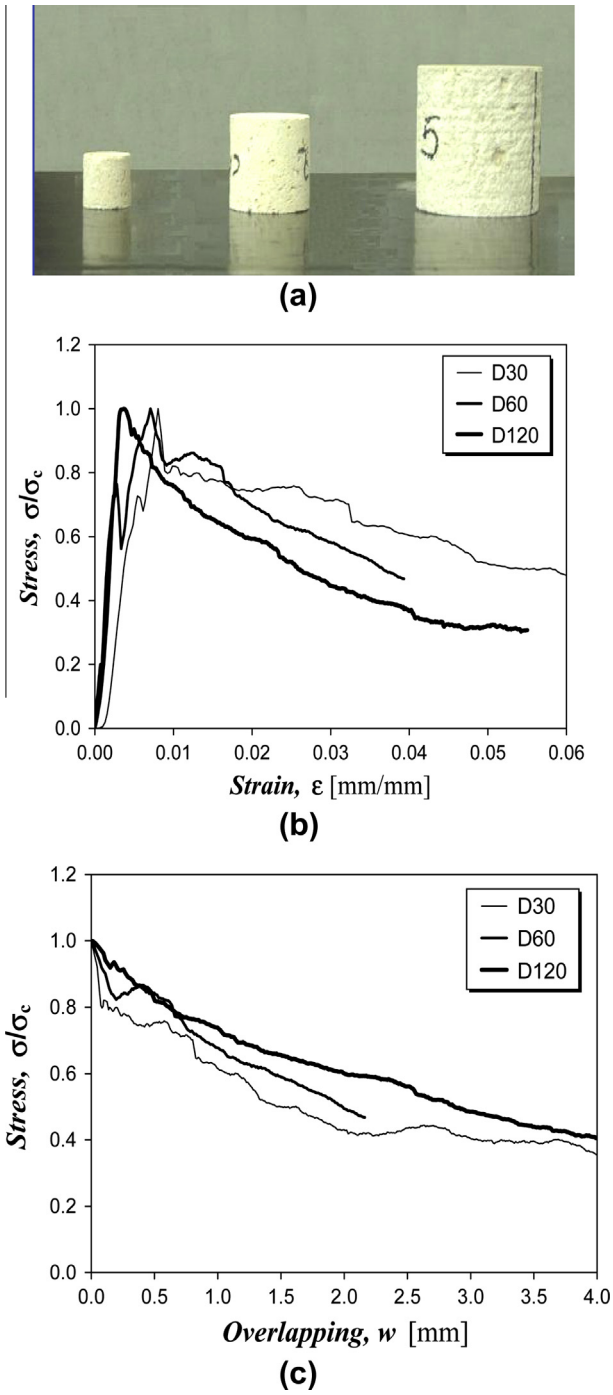

Fig. 5. Compression tests on rock specimens by Carpinteri et al. [20] (a); stress vs. strain diagrams (b); overlapping law diagrams (c).

$$B = \frac{S_E}{\varepsilon_c \lambda} \leqslant \frac{1}{2.3}, \tag{2}$$

where $\lambda = l/d$ is the specimen slenderness, ε_c is the elastic strain recovered during the softening unloading, and

$$S_E = \frac{G_c}{\sigma_c d} \tag{3}$$

is the energy brittleness number in compression, proposed by Carpinteri et al. [6].

For the sake of example, the stress vs. overlapping displacement curves obtained from the experiments on concrete specimens having different sizes and slendernesses by Ferrara and Gobbi [19] are shown in Fig. 4 (see Ref. [7] for an extended model validation on different concrete-like materials). The stress–strain curves reported in Fig. 4b clearly evidence that the pre-peak elastic regime results to be independent of any geometrical parameters, whereas the post-peak regime is largely influenced by the slenderness and the scale of the specimen. Therefore, the stress–strain relationship cannot be assumed as a material property. On the contrary, the stress–displacement curves collapse onto a very narrow band (see Fig. 4c), demonstrating that the σ–w relationship is able to provide a scale-invariant constitutive law. From a practical point of view, the post-peak localised interpenetration, w, is computed from the total shortening of the specimen, δ by subtracting the elastic contribution εl, according to Eq. (1). Similar results are obtained for the limestone specimens extracted from a pillar of the Syracuse Cathedral [20] (Fig. 5). The substantial collapse of the curves onto a narrow band obtained in comparison to the stress vs. strain diagrams, extends the applicability of the overlapping law, originally proposed for concrete, also to rock materials.

3. Experimental tests

The experimental investigation herein presented focuses on the mechanical response of cylindrical specimens of different heterogeneous materials, such as rocks and concrete, subjected to uniaxial compression tests. As regards the rock specimens, three different types have been tested: Luserna stone, Carrara marble, and Syracuse limestone. Luserna stone is a lamellar metamorphic rock deriving from a granitoid protolith quarried in Piedmont (Italy). Carrara marble is a type of white or blue-grey calcite marble quarried in Carrara (Tuscany, Italy) popular for use in sculpture and building décor. Syracuse limestone is a porous calcareous stone obtained from quarries in the area of Plemmirio (Sicily, Italy). All the three rock samples have a slenderness $\lambda = 2.0$, being the diameter $d = 50$ mm and the length $l = 100$ mm. As regards the concrete specimen, a normal strength concrete has been considered, having an average compressive strength equal to 45 MPa. The slenderness of the sample is again $\lambda = 2.0$, though the diameter is equal to 100 mm and the length to 200 mm.

On the basis of previous experiences, a very brittle behaviour, characterised by a snap-back instability, was expected for the Luserna specimen, an intermediate response for the Carrara marble and the normal concrete samples, and a ductile behaviour for the limestone. On the other hand, a correct evaluation of the dissipated and released energies during the complete loading process can be done only if the load–displacement curve is fully detected, post-peak branch included. To this purpose, the loading processes of the Luserna stone, the Carrara marble and the concrete specimens have been controlled by the circumferential strain, that results to be a monotonic increasing function of time, even in case of global brittle behaviour. An extensometer attached to the ends of a linked chain with roller at each hinge was placed around the cylinders at mid-height, measuring the circumferential expansion. Such a device is particularly effective in controlling the post-peak phase for specimens with slenderness of about 2.0, characterised by a splitting failure mode. The velocity of the circumferential expansion has been set equal to 1×10^{-3} mm/s for the Luserna specimen, to 5×10^{-4} mm/s for the Carrara specimen, and 2×10^{-3} mm/s for the concrete sample. Due to the expected ductile behaviour for the limestone specimen, its loading process was controlled by the longitudinal displacement (piston stroke). In this case, a constant piston velocity was imposed, equal to 1×10^{-3} mm/s. In all the cases the load has been applied by means of rigid platens without interposing friction-reducer devices. At this regard, it is worth noting that there is vast amount of literature confirming that the friction effects are very limited in the case of sample slendernesses equal to or larger than 2.0. During the tests, each specimen was monitored by applying a piezoelectric transducer on the sample surface in order to detect acoustic emissions emerging from the compression process. The sensitivity range for the transducer is from 50 to 800 kHz, making possible the detection of high-frequency AEs. The sampling frequency of recording waveforms was set to 1 Msample/s. The AE waves, captured by the sensors, were amplified with 60 dB gain before they have been processed, setting the acquisition threshold level up to 2 mV.

The load vs. circumferential and longitudinal displacement curves obtained from the tests are shown in Figs. 6a–9a. The mechanical response of the Luserna stone is highly unstable in terms of load vs. axial displacement, whereas a global softening behaviour with the presence of several peaks and valleys is obtained in terms of load vs. circumferential expansion (Fig. 6a). Carrara marble and normal concrete are characterised by a load vs. axial displacement with perfect vertical drop after the peak load and a smooth softening curve in the load vs. circumferential expansion diagram (Figs. 7a and 8a). Finally, a ductile response in the load vs. axial displacement diagram has been obtained for the Syracuse limestone specimen (Fig. 9a).

As far as the acoustic emission activity is concerned, in the Luserna stone specimen it is mainly concentrated in the post-peak stage, as clearly evidenced by the cumulated number of AE and the AE count rate diagrams shown in Fig. 6b and c. The cumulated number of AE events referred to the post-peak regime is about 3200. Analogously, also the Carrara marble and the concrete samples have exhibited significant AE events in the post-peak, even if the cumulated numbers are one order of magnitude lower than that of the Luserna stone (300 for marble and 160 for concrete, as can be deduced from Figs. 7 and 8). On the contrary, almost all of the AE events in the limestone specimen has been detected in the pre-peak stage, as shown in Fig. 9b. As regards the post-peak regime, the cumulated number of AE is around 400.

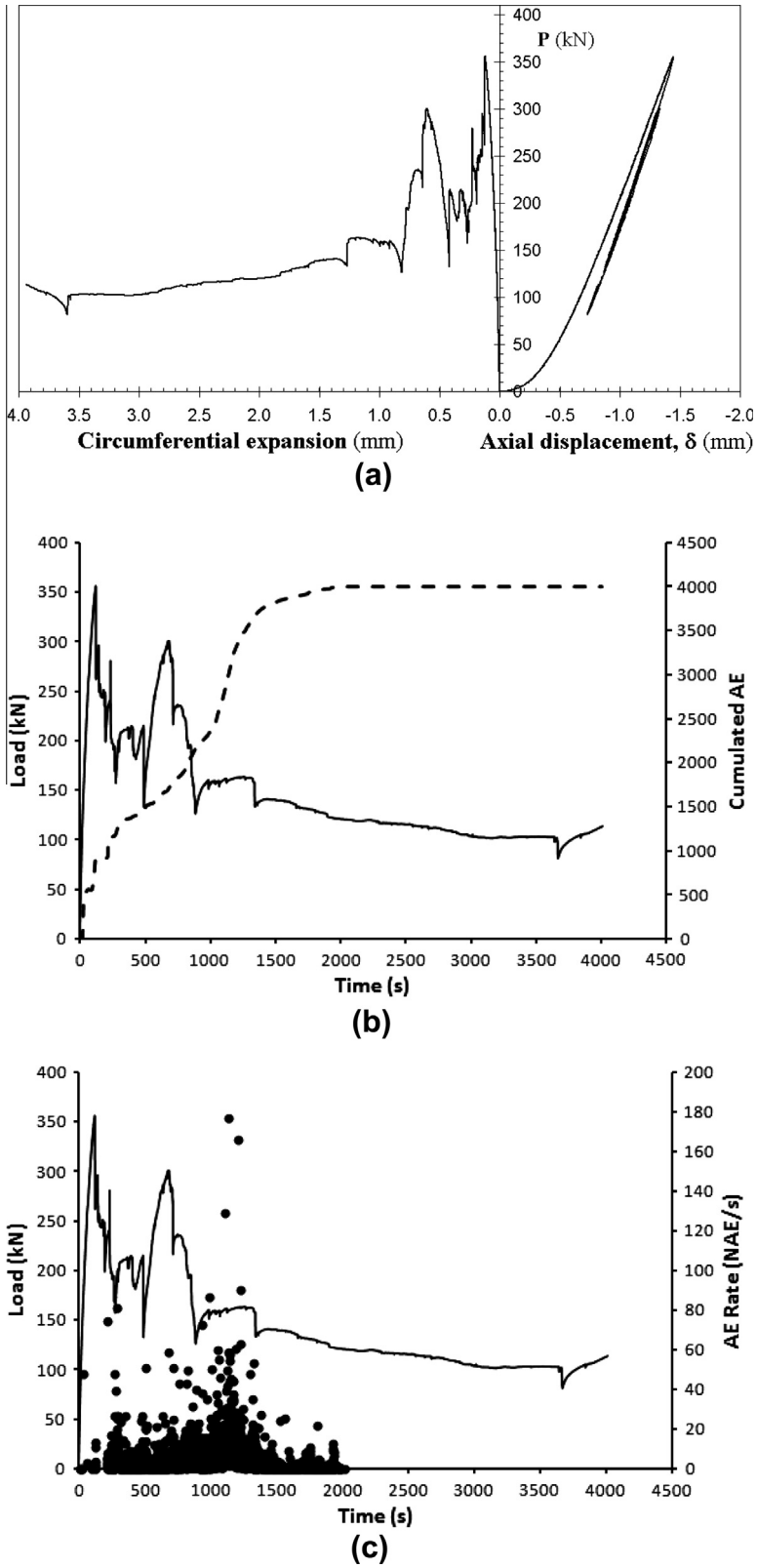

Fig. 6. Compression test on the Luserna stone specimen (d = 50 mm, l = 100 mm): (a) load vs. circumferential expansion and longitudinal displacement diagrams; (b) load vs. time curve with cumulated number of AE and, (c) AE count rate.

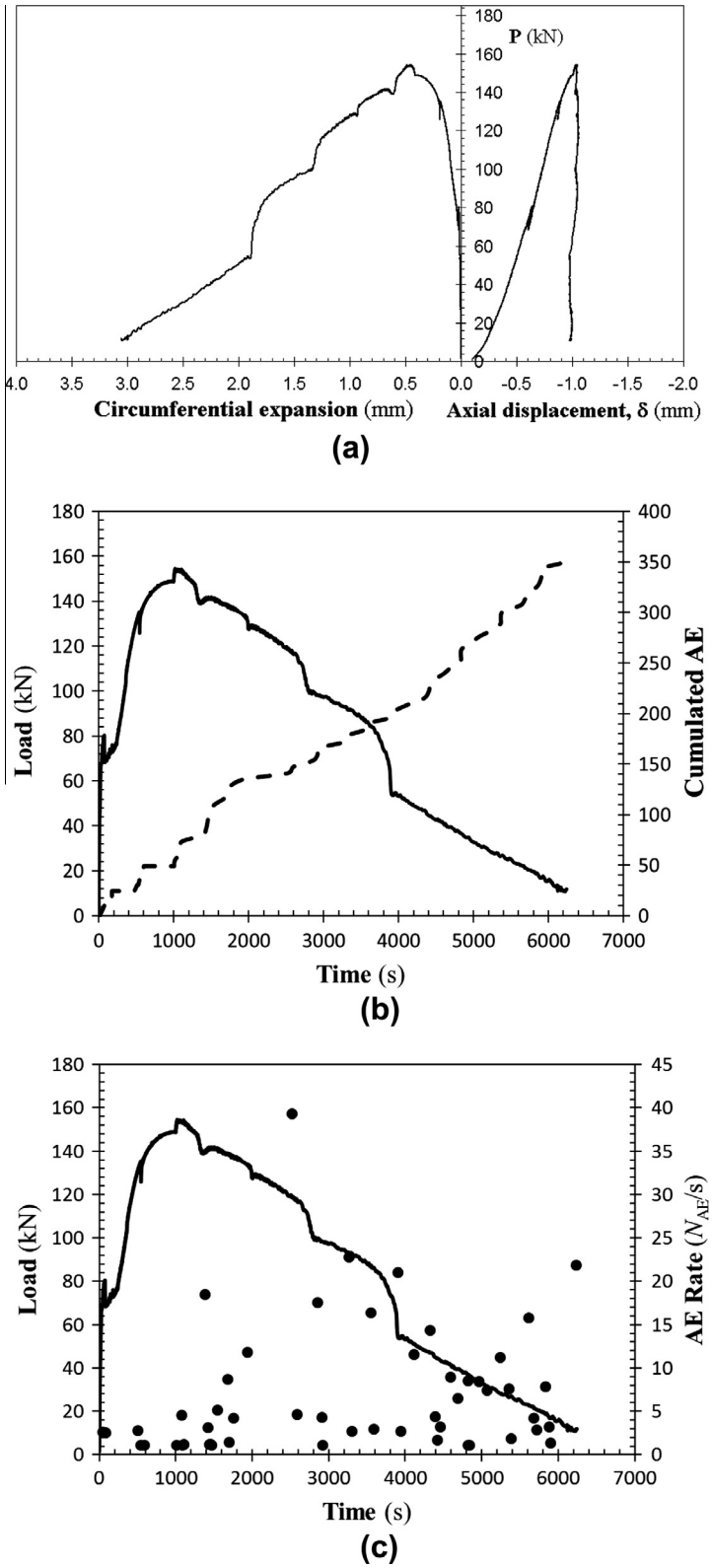

Fig. 7. Compression test on the Carrara marble specimen (d = 50 mm, l = 100 mm): (a) load vs. circumferential expansion and longitudinal displacement diagrams; (b) load vs. time curve with cumulated number of AE and, (c) AE count rate.

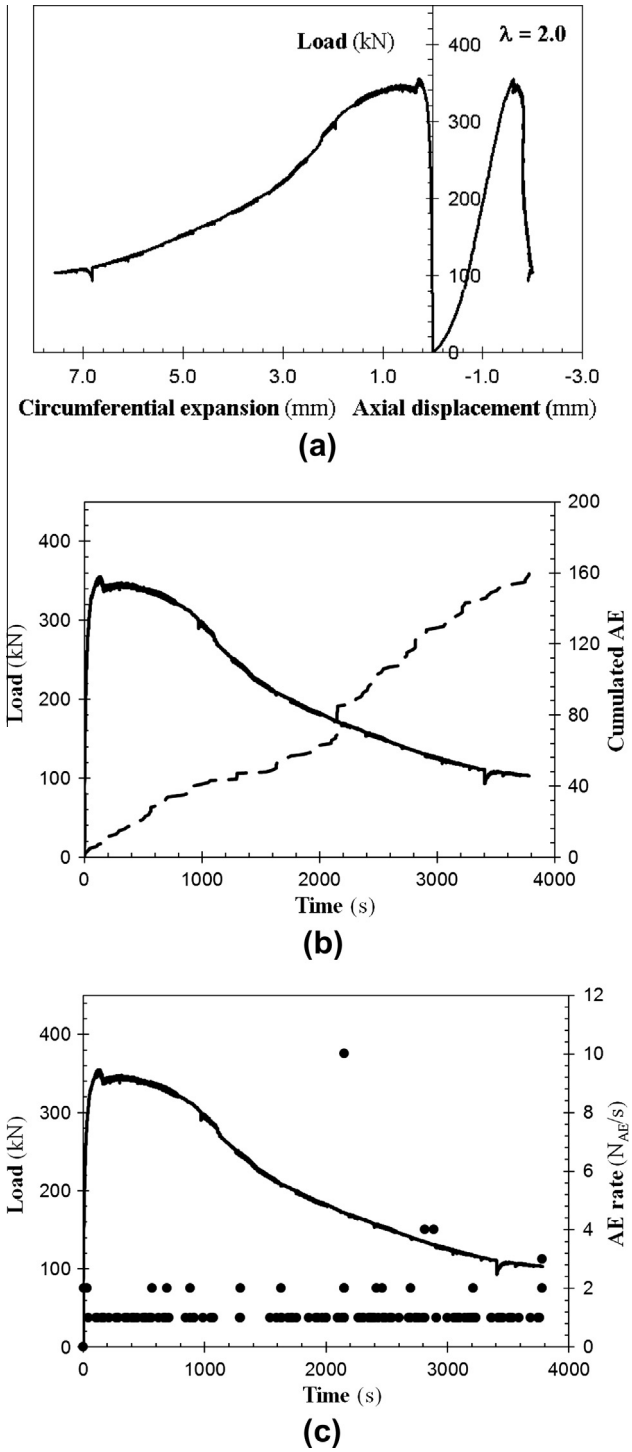

Fig. 8. Compression test on the concrete specimen with slenderness $\lambda = 2.0$ ($d = 100$ mm, $l = 200$ mm): (a) load vs. circumferential expansion and longitudinal displacement diagrams; (b) load vs. time curve with cumulated number of AE and, (c) AE count rate.

4. Stability of the loading process and energy release

The mechanical responses obtained for the considered materials can be referred to the three cases shown in Fig. 3: normal softening, vertical drop and snap-back instability. Such a transition can be obtained either by varying the specimen geom-

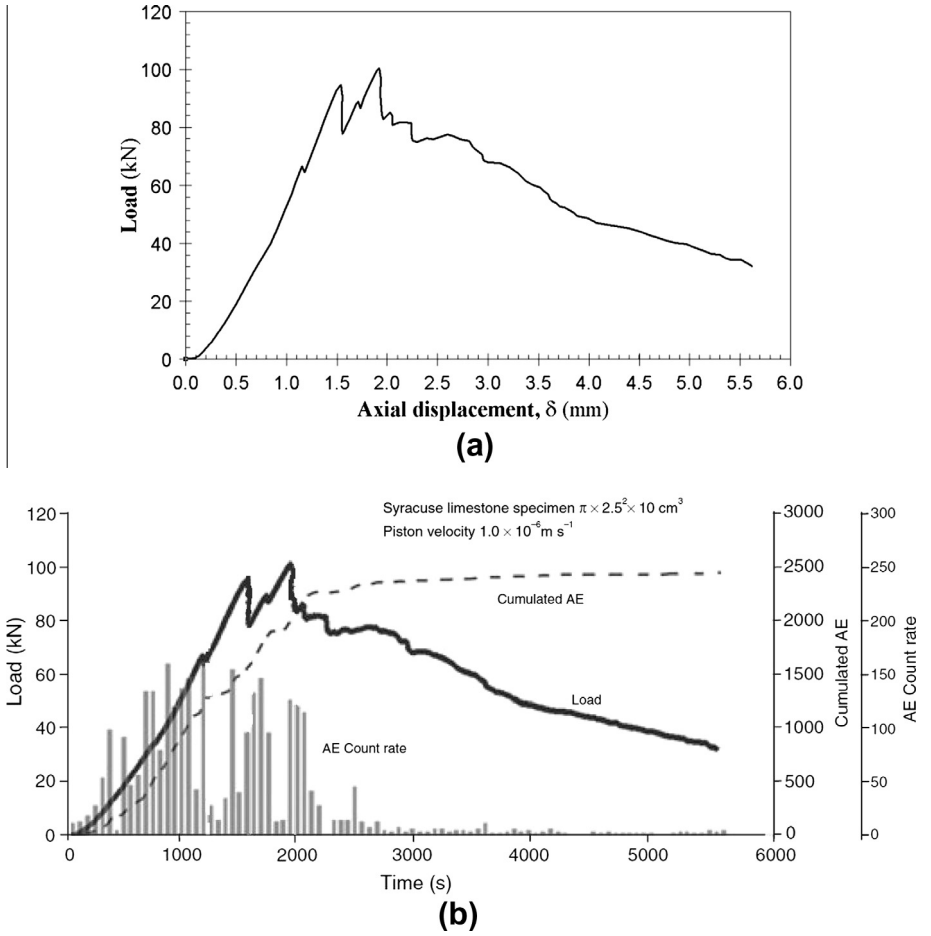

Fig. 9. Compression test on the Syracuse limestone specimen (d = 50 mm, l = 100 mm): (a) load vs. longitudinal displacement diagram, and (b) load vs. time curve with cumulated number of AE and AE count rate.

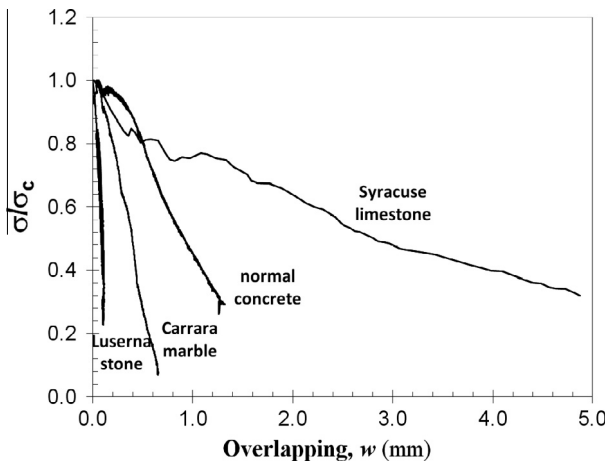

Fig. 10. Overlapping constitutive laws for Luserna stone, Carrara marble, Syracuse limestone and normal concrete specimens.

etry, the material being the same, or, as in this study, by varying the material properties and keeping the geometric parameters constant. The procedure described in Section 2 has been used to derive the overlapping laws for the four considered materials. They are shown in Fig. 10, in terms of normalised stress vs. overlapping displacement. The values of the strength,

Table 1
Mechanical parameters for the four considered materials.

	σ_c (MPa)	ε_c	w_{cr} (mm)	G_C (N/mm)	s_E	B	$G_C \times$ Area (J)	ΔE (J)
Luserna stone	168	0.0105	0.12	13.90	0.0016	0.079	29.51	186.40
Carrara marble	75	0.0080	0.60	25.35	0.0065	0.410	49.57	57.75
Normal concrete	45	0.0077	1.60	43.00	0.0095	0.620	337.72	272.14
Syracuse limestone	51	0.0180	6.00	165.00	0.0650	1.889	323.89	85.42

the critical interpenetration displacement and the crushing energy are reported in Table 1. The crushing energy G_C has been evaluated as the area beneath the overlapping law comprised between the peak stress, σ_c, and a residual stress equal to $0.2\sigma_c$. On the basis of these mechanical properties and the specimen diameter, the energy brittleness number s_E has been computed for each specimen. The lowest value is that of the Luserna stone sample, equal to 0.0016, and the largest one is that of the Syracuse limestone sample, equal to 0.065. The marble and the concrete specimens present intermediate values for s_E, equal to 0.0065 and 0.0095. The values of the parameter B, defined in Eq. (2), are also reported in Table 1. They completely agree with the critical condition defined by Eq. (2): snap-back instability for $B < 0.43$, and normal softening for $B > 0.43$. The Carrara marble specimen, characterised by a vertical drop in the load–displacement diagram, has $B = 0.41$.

According to the OCM, the energy absorbed in the post-peak phase by the damaging process is equal to the crushing energy times the transversal cross section of the specimen. The values for the four samples are reported in Table 1. On the other hand, the elastic strain energy at the peak load, ΔE, represents the maximum energy stored in the specimen, that will be partially absorbed and partially released during the post-peak phase. As can be deduced from the results reported in Table 1, the Luserna specimen releases an energy equal to 156.89 J, and the Carrara sample to 8.18 J. On the contrary, the concrete and the limestone specimens requires a supplementary amount of energy, to be provided by the testing machine, for the advancement of the post-peak damaging process (65.58 J and 238.47 J, respectively). As regards the Carrara marble specimen, the value of the crushing energy multiplied by the cross-sectional area is not exactly equal to ΔE, even if the load–displacement diagram has a vertical drop, because the crushing energy is computed up to the residual stress $\sigma_r = 0.2\sigma_c$, and not up to a complete failure. The obtained experimental results evidence that the AE activity in the post-peak phase can be directly related to the energy release. The largest number of AE events, in fact, has been detected for the Luserna stone specimen, which, according to the previous calculations, is that releasing the largest amount of energy. Limited AE events have been detected from the Carrara marble specimen, for which the accumulated and the absorbed energies are almost the same, whereas a low AE activity in the post-peak regime has been observed for the limestone specimen.

5. AE analysis to discriminate the failure mechanisms

All the specimens described in the previous sections, having a slenderness equal to 2.0, were characterised by a splitting failure, i.e. dominant Mode I failure. In order to verify the capability of the AE in discriminating the types of failure, another specimen of normal concrete, having a diameter equal to 100 mm and slenderness equal to 1.0, has been tested. In this case, the loading process has been controlled by the circumferential strain up to the maximum displacement for the extensometer (point A in Fig. 11a and b), then, the test control has been switched to the piston stroke.

The load vs. circumferential expansion and the load vs. axial displacement curves for the specimen having slenderness equal to 1.0 are shown in Fig. 11a. The obtained overall behaviour results to be more ductile then that of the specimen with slenderness equal to 2.0, the post-peak regime being characterised by a normal softening response. Such a result is consistent with the prediction given by the parameter B defined in Eq. (2). In this case, in fact, it is equal to 1.24, twice the value referred to the previous specimen. However, the two failure mechanisms are very different: a shear failure with several slip bands characterises the specimen with $\lambda = 1.0$, whereas a splitting failure is obtained for the specimen with $\lambda = 2.0$. Furthermore, the behaviour of the specimen less slender is also affected by the friction between loading platens and specimen ends. Such an effect yields to an increase in the load carrying capacity and in the energy dissipation.

In this section, AE parameters such as rise time, peak amplitude and average frequency are analysed in order to classify active cracks. In particular, the ratio of the rise time (expressed in ms) to the peak amplitude (expressed in V) of each signal are used to calculate the Rise Angle (RA) value [8–10,16]. The shape of the AE waveforms is typical of the fracture mode (Fig. 12): shear events are characterised by long rise times and usually high amplitudes [17,21,22], whereas low rise time values are typical of tensile crack propagations [21,22]. Another parameter used to characterise the cracking mode is the Average Frequency (AF) expressed in kHz. The AF values are obtained from the AE ringdown count divided by the duration time of the signal. The AE ringdown count corresponds to the number of threshold crossings within the duration time. In general, the shift from higher to lower values of AF could indicate the shift of the cracking mode from tensile to shear [17]. Nevertheless, when a cracking process involves the opening of large cracks (Mode I), the frequency attenuation must be a function of this discontinuity. In other words, in this case the wavelength of the AE signals needs to be larger for the crack opening to be overcome, and the shift of the frequencies from higher to lower values could support also a dominant tensile cracking mode [12,23].

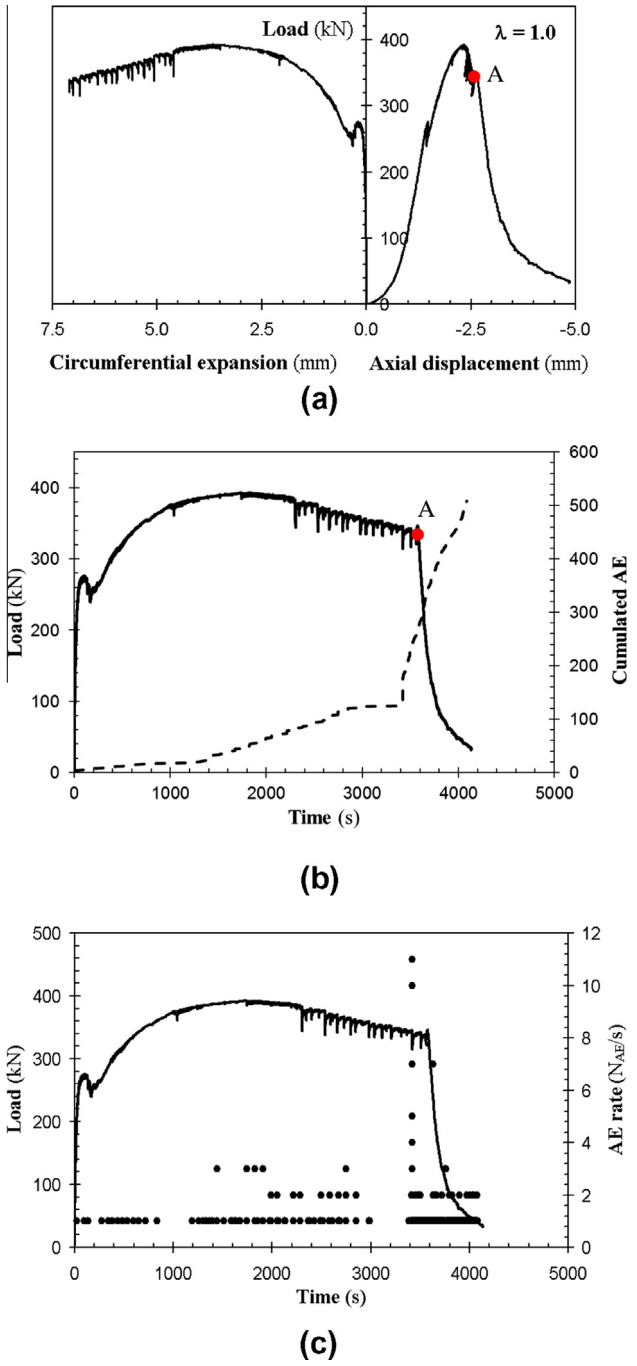

Fig. 11. Concrete specimen with slenderness $\lambda = 1.0$ ($d = 100$ mm, $l = 100$ mm): (a) load vs. circumferential expansion and longitudinal displacement diagrams; (b) load vs. time curve with cumulated number of AE and, (c) AE count rate.

In the case of $\lambda = 1.0$, the cumulative number of AE events at the end of the test is larger than the case with $\lambda = 2.0$ (see Fig. 11b compared to Fig. 8b), representing a higher energy dissipation due to friction. The AE average frequencies decrease from 230 kHz to 190 kHz during the loading test. The load process involves a small shift in frequencies from higher to lower values (Fig. 13a) and a significant increase in RA values after the peak load is come out (Fig. 13b). Therefore a dominant presence of shear cracks seems to lead the damage evolution up to the final collapse. The analysis of the energy content obtained by the AE signals (Fig. 13c), calculated as proportional to the envelope of the signal waveform [8], verifies that the damage evolution carries more powerful signals after the peak load, when the final collapse is approaching. During this test, the amount of released AE signals energy is estimated as 1460 10^{-3} ms V.

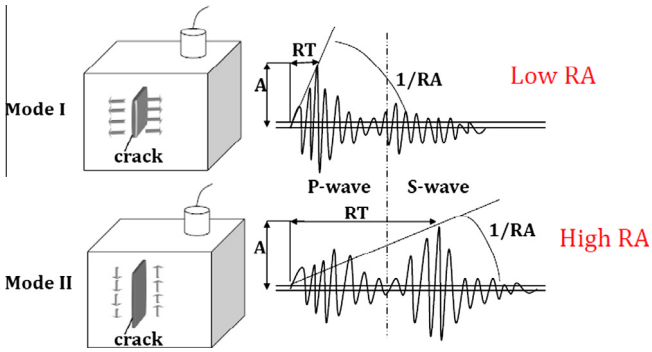

Fig. 12. Typical waveforms of tensile and shear events. *A* is the amplitude and RT the Rise Time (time between the onset and the point of maximum amplitude) of the waveforms [22].

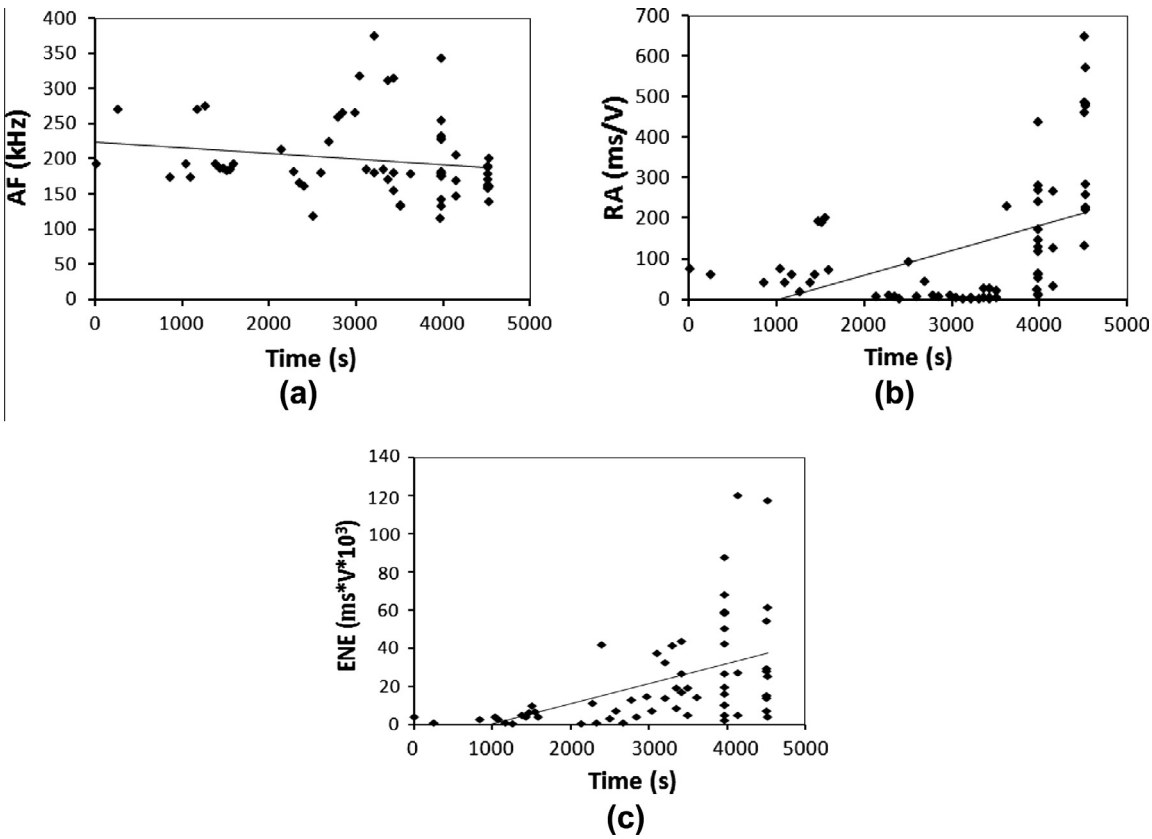

Fig. 13. Concrete specimen with slenderness $\lambda = 1.0$: (a) AF values vs. time; (b) RA values vs. time; (c) AE signals energy vs. time.

As regards the specimen with slenderness $\lambda = 2.0$, the AE average frequencies decrease from 100 kHz to 50 kHz during the loading test (Fig. 14a). The loading process involves a shift in frequencies from higher to lower values and a significant decrease in RA values after the peak load (Fig. 14b). Therefore a dominant presence of tensile cracks seems to lead the damage evolution up to the final collapse. Due to the slenderness of the specimens and the failure mode shown during the experiment (a single large subvertical crack), the shift in frequencies tends to very low values. As a matter of fact, for high frequency waves it is possible to propagate only through small inhomogeneities, whereas low frequency waves can propagate also through large inhomogeneities [12,23]. From the analysis of the energy content obtained from AE signals (Fig. 14c), also in this case it is verified that the damage evolution carries more powerful signals after the peak load. The amount of released AE signals energy at the end of the test, estimated as 680 10^{-3} ms V, is lower than the previous case.

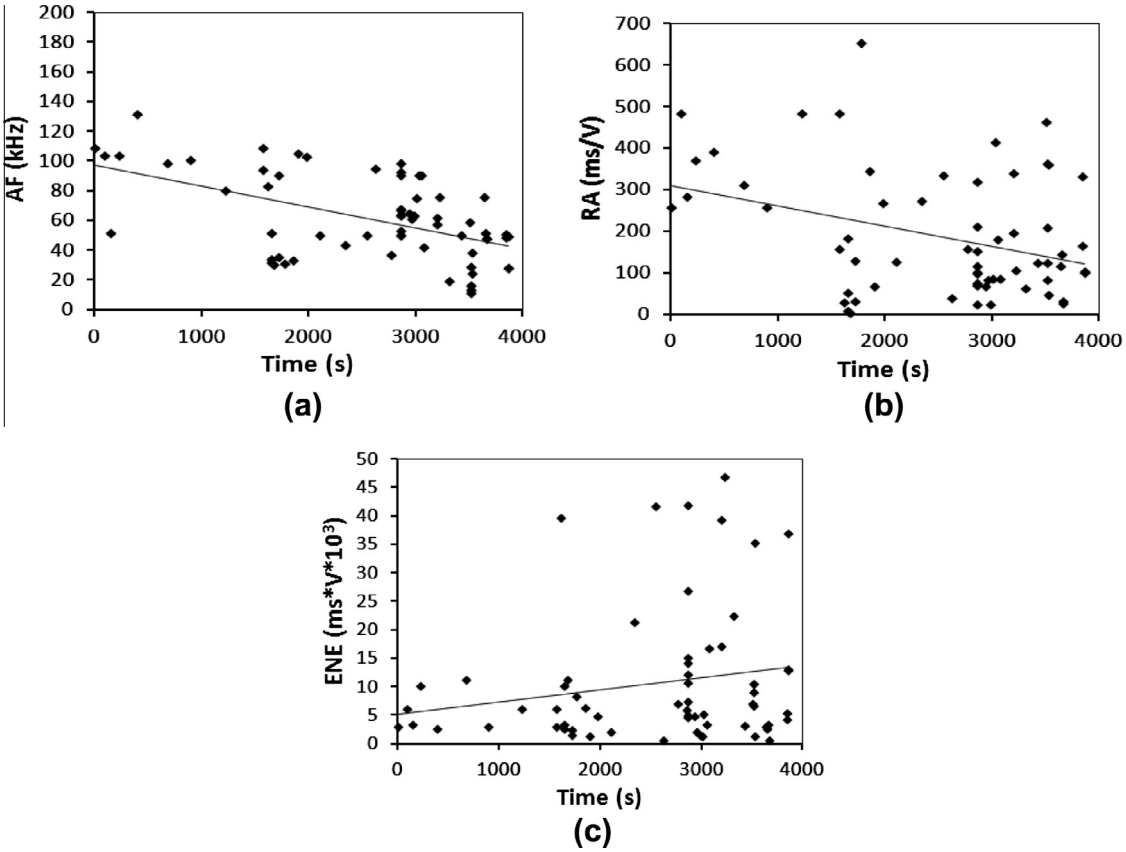

Fig. 14. Concrete specimen with slenderness $\lambda = 2.0$: (a) AF values vs. time; (b) RA values vs. time; (c) AE signals energy vs. time.

6. Conclusions

In the present paper, the results of compression tests carried out on cylindrical specimens of concrete and different rock types have been analysed considering the stability of the loading process and the relationship between absorbed and released energy during the post-peak phase. The following main conclusions may be drawn:

(1) The use of the circumferential strain as controlling parameter of the compression tests permits the post-peak branch to be detected, also for a very brittle material such as Luserna stone. This is fundamental to derive the scale-invariant overlapping constitutive law by applying the inverse of Eq. (1), that, in its turn, is useful to define the structural brittleness, represented by the dimensionless parameter B defined by Eq. (2). In particular, for the considered specimen dimensions, Luserna stone results to be the most brittle, and Syracuse limestone the most ductile.
(2) The results depicted in Figs. 6–9 show how the number of AE events in the post-peak regime is proportional to the released energy, that is evaluated as the difference between the elastic strain energy at the peak load and the energy absorbed by the crushing process.
(3) The AE results obtained from compression prove that the variation of the AE parameters during the loading process strictly depends on the specimen damage: a decrease in the frequency coupled to low RA values suggest a Mode I crack propagation, whereas a decrease in the frequency coupled to high RA values are obtained in case of Mode II crack propagation. All the monitored damage processes display an increase of AE signal energy content approaching the final failure.

Acknowledgements

The financial supports provided by the Ministry of University and Scientific Research (MIUR) to the project "Advanced applications of Fracture Mechanics for the study of integrity and durability of materials and structures", and by the Regione Piemonte to the RE-FRESCOS project: "Preservation, safeguard and valorisation of masonry decorations in the architectural

historical heritage of Piedmont", are gratefully acknowledged. The authors wish also to thank Eng. F. Accornero for his active collaboration in the execution of the compression tests under circumferential displacement control.

References

[1] Carpinteri A, Corrado M, Lacidogna G. Three different approaches for damage domain characterization in disordered materials: Fractal energy density, *b*-value statistics, renormalization group theory. Mech Mater 2012;53:15–28.
[2] Hudson JA, Brown ET, Fairhurst C. Shape of the complete stress–strain curve for rock. In: Cording EJ, editor. Stability of rock slopes (proceedings of the 13th symposium on rock mechanics). New York: American Society of Civil Engineers; 1972. p. 773–95.
[3] Kotsovos MD. Effect of testing technique on the post-ultimate behaviour of concrete in compression. Mater Struct 1983;16:3–12.
[4] van Mier JGM. Strain softening of concrete under multiaxial compression. PhD Thesis. The Netherlands: Eindhoven University of Technology; 1984.
[5] Jansen DC, Shah SP. Effect of length on compressive strain softening of concrete. J Eng Mech 1997;123:25–35.
[6] Carpinteri A, Corrado M, Mancini G, Paggi M. The Overlapping Crack Model for uniaxial and eccentric concrete compression tests. Mag Concr Res 2009;61:745–57.
[7] Carpinteri A, Corrado M, Paggi M. An analytical model based on strain localization for the study of size-scale and slenderness effects in uniaxial compression tests. Strain 2011;47:351–62.
[8] RILEM Technical Committee TC212-ACD. Acoustic Emission and related NDE techniques for crack detection and damage evaluation in concrete: measurement method for acoustic emission signals in concrete. Mater Struct 2010;43:1177–1181.
[9] RILEM Technical Committee TC212-ACD. Acoustic Emission and related NDE techniques for crack detection and damage evaluation in concrete: test method for damage qualification of reinforced concrete beams by Acoustic Emission. Mater Struct 2010;43:1183–1186.
[10] RILEM Technical Committee TC212-ACD. Acoustic Emission and related NDE techniques for crack detection and damage evaluation in concrete: test method for classification of active cracks in concrete by Acoustic Emission. Mater Struct 2010;43:1187–1189.
[11] Ohtsu M. The history and development of acoustic emission in concrete engineering. Mag Concr Res 1996;48:321–30.
[12] Carpinteri A, Lacidogna G, Pugno N. Structural damage diagnosis and life-time assessment by acoustic emission monitoring. Eng Fract Mech 2007;74:273–89.
[13] Carpinteri A, Lacidogna G, Niccolini G, Puzzi S. Critical defect size distributions in concrete structures detected by the acoustic emission technique. Meccanica 2008;43:349–63.
[14] Carpinteri A, Lacidogna G, Puzzi S. Prediction of cracking evolution in full scale structures by the b-value analysis and Yule statistics. Phys Mesomech 2008;11:260–71.
[15] Weiss J, Marsan D. Three-dimensional mapping of dislocation avalanches: clustering and space/time coupling. Science 2003;299:89–92.
[16] Grosse C, Ohtsu M. Acoustic emission testing. Springer; 2008.
[17] Ohno K, Ohtsu M. Crack classification in concrete based on acoustic emission. Constr Build Mater 2010;24:2339–46.
[18] Okubo S, Nishimatsu Y. Uniaxial compression testing using a linear combination of stress and strain as the control variable. Int J Rock Mech Min Sci Geomech 1985;22:323–30 [Abstract].
[19] Ferrara G, Gobbi ME. Strain softening of concrete under compression, Report to RILEM Committee 148 SCC, ENEL-CRIS Laboratory, Milano, Italy; 1995.
[20] Carpinteri A, Lacidogna G, Manuello A. The *b*-value analysis for the stability investigation of the ancient Athena temple in Syracuse. Strain 2011;47:e243–53.
[21] Soulioti D, Barkoula NM, Paipetis A, Matikas TE, Shiotani T, Aggelis DG. Acoustic emission behavior of steel fibre reinforced concrete under bending. Constr Build Mater 2009;23:3532–6.
[22] Aggelis DG. Classification of cracking mode in concrete by acoustic emission parameters. Mech Res Commun 2011;38:153–7.
[23] Landis EN, Shah SP. Frequency-dependent stress wave attenuation in cement-based materials. J Eng Mech 1995;121:737–43.